Electronic Supplementary Material (ESI) for Journal of Materials Chemistry A.

Supplementary Information

Anisotropic conductive shape-memory aerogel as adaptive reprogrammable wearable electronics for accurate long-term pressure sensing

Jinhui Huang, Yilei Wang, Jing Guo, Shanshan Wu, Hui Xie, Shaobing Zhou**

Key Laboratory of Advanced Technologies of Materials, Ministry of Education of China, School of Materials Science and Engineering, Southwest Jiaotong University, Chengdu 610031, P. R. China.

* Corresponding authors:

E-mail: huixie@swjtu.edu.cn, shaobingzhou@swjtu.edu.cn

Experimental section

Materials

Polyethylene glycol (PEG_{4000}, M_n = 4000 g/mol) was purchased from Sinopharm Chemical Reagent Co., Ltd. (China). Poly (ethylene glycol) diacrylate ($PEGDA_{600}$, M_n = 600 g/mol), Ammonium persulfate (APS), *N, N, N', N'*-Tetramethyl ethylenediamine (TEMED) and acryloyl chloride were purchased from Aladdin Reagent Co., Ltd. (China). Dichloromethane (CH_2Cl_2), diethyl ether, potassium carbonate (K_2CO_3) and calcium hydride (CaH_2) were purchased from Kelong Reagent Corp. (Chengdu, China). Aminoated multi-walled carbon nanotubes (A-CNTs, OD: 8-15nm, Length: 0.5-2μm) and water dispersant (TNWDIS) were purchased from Chengdu Organic Chemicals Co., Ltd. (China).

Synthesis of Poly (ethylene glycol) diacrylate (PEGDA)

PEG_{4000} (20.0g, 0.005 mol) was dissolved in anhydrous CH_2Cl_2 (100 mL, dried by CaH_2), and K_2CO_3 (3.455 g, 0.025 mol) was added as the acid-binding agent. The reaction solution was stirred at room temperature for 0.5 h. Then, acryloyl chloride (2.03 mL, 50 mmol) was added to 20 mL of anhydrous CH_2Cl_2 and added to the former reaction dropwise, and the reaction was kept stirring at room temperature for 48 h. Upon the completion of the reaction, the reaction mixture was extracted to remove excess acryloyl chloride and inorganic salts. The mixture was concentrated back to 20 mL by rotation evaporation and then precipitated by cold diethyl ether. Finally, the resulting precipitate was filtered under reduced pressure. The white solid ($PEGDA_{4000}$) was obtained and dried under vacuum at room temperature to a constant weight.

Preparation of A-CNTs dispersion

Firstly, 1 g of TNWDIS was dissolved in 32 g of deionized (DI) water. Then, 1g A-CNT was added and stirred for 0.5 h and used an ultrasonic cell disruptor to sonicate for 2 h in an ice bath. The content of the prepared A-CNTs dispersion was 3 wt%.

Nuclear Magnetic Resonance (NMR)

^{1}H-NMR spectra of PEGDA in $CDCl_3$ were recorded by a Bruker AM-300 MHz spectrometer (Bruker, Germany) at room temperature using tetramethylsilane as an internal reference.

Fourier transform infrared spectroscopy (FT-IR)

All the samples were tested by using Nicolet 5700 (Nicolet) with a resolution of 4 cm^{-1}, and the FT-IR spectra were obtained by 32 scans in the range of 4000-500 cm^{-1}.

Swelling testing

The sample (m_o) was soaked in chloroform for 48 h. After being dried, the insoluble residue (m_d) was weighted, and the gel content (G) was calculated according to equation (1). For each group, three samples were tested to obtain the mean value.

$$G = \frac{m_d}{m_o} \times 100\% \quad (1)$$

Measurement of apparent density of the aerogels

The apparent volumetric mass density (ρ_0) of aerogels were calculated according to equation (2),

$$\rho_0 = \frac{m}{V_0} \quad (2)$$

where m and V_0 were the weight and volume of the aerogel measured with an analytical balance and vernier caliper, respectively. Each sample was tested for three times to obtain the mean value.

Measurement of porosity of the aerogels

The porosity of aerogel was calculated by equations (3)-(4),

$$Porosity = \left(1 - \frac{\rho}{\rho_s}\right) \times 100\% \quad (3)$$

$$\rho_s = \frac{1}{\frac{W_{PEG}}{\rho_{PEG}} + \frac{W_{A-CNT}}{\rho_{A-CNT}}} \times 100\% \quad (4)$$

where ρ and ρ_s are the densities of the series of aerogels and typical PEG/A-CNTs solid materials respectively, $W_{PEG}$and W_{A-CNT} are the weight fractions of PEG and A-CNTs respectively, and ρ_{PEG} and ρ_{A-CNT} are the densities of PEG and A-CNTs respectively. Here, ρPEG4000 is 1.13 g/cm^3 and ρA-CNT is 0.27 g/cm^3. Each sample at least tested three times to obtain the mean value.

Water contact angle (WCA) testing

WCA was measured with a contact angle meter (DSA 100, Kruss, Germany) using 5 μL of deionized water at room temperature. Each WCA was tested for at least three different locations to obtain the mean value.

Scanning Electron Microscopy (SEM)

Surface morphologies and microstructures of the aerogels were observed by SEM (Apreo 2 SEM, Thermo Fisher Scientific, USA) at an acceleration voltage of 5-10 kV. The aerogels were fractured by liquid nitrogen in the axial and radial respectively and sputtered with gold before testing.

Investigation of mechanical properties

The mechanical properties of the aerogels (size: 10mm×10mm×8mm) were assessed using a

commercial tester (INSTRON 5965, USA) at room temperature. Before testing, a small force (0.2 N) was applied in advance to ensure the sample closely contact with the two indenters. The strain rate is controlled at 5 mm/min, and the cyclic loading is performed with a strain rate of 50 mm/min.

Differential Scanning Calorimetry (DSC)

The thermal properties of the aerogels were characterized by using a DSC-2500 instrument (TA, USA). The samples were firstly heated to 80 °C and isothermal for 3 min to eliminate thermal history. Subsequently, the sample was cooled to -20 °C and reheated to 80 °C in successive cycles at a rate of 5 °C/min. The heating and cooling curves were recorded and the crystallization and melting behavior were analyzed.

Applications of aerogel in human physiological activity detection

To demonstrate the routine application of aerogel sensor, we fixed aerogel sensor on the skin surface of different parts of the human body with PU medical tape, such as throat, wrist, knee, etc., to detect human physiological activities. Human body activities cause compression of aerogel, and reflected by resistance changes recorded by a digital multimeter (DMM6500, Keithley, USA).

Models for investigations of long-term wearable sensing

Model 1: Tree branch bending

The SMAFE was pre-heated at 70 °C and curled on the ginkgo tree branch at this temperature, followed by a cooling procedure at -10 °C for a complete fixation. After that, the model was studied at room temperature, and bending degrees of the tree branch were reflected by resistance changes recorded by a digital multimeter (DMM6500, Keithley, USA).

Model 2: Pipeline expansion

The SMAFE was fixed onto a rubber hose (d = 6 mm) using shape-memory to simulate the expansion and deformation of the hose when it was blocked in a ventilated environment. Once the rubber hose was filled with nitrogen using a nitrogen tank, plugging another side of the hose would generate massive storage of gas in the tube, leading to the expansion and deformation of the hose. The expansion was examined by a pressure sensing mechanism and recoded by DMM6500.

Model 3: Finger movement

The SMAFE in strip shape (thickness: 4.20 mm) was heated and compressed to a thinner one

(thickness: 1.08 mm), followed by a cooling procedure to fix this temporary shape. Then, the deformed film was connected end to end by an adhesive to form a ring-like shape (inner diameter: 17.8 mm, outer diameter: 20.67 mm). The ring-like SMAFE was then put on the finger of a prosthetic hand with a diameter of ~13.6mm, and heated by an oven (household hairdryer was also applicable) to activate the recovery process until the SMAFE self-fitly attached to the finger. At this stage, the inner and outer diameters of the ring-like SMAFE became 13.65 and 22.15 mm respectively, and this could be regarded as the accomplishment of wearing. Finally, the resistance changes caused by the finger bending at different angles were recorded by DMM6500.

Model 4: Wrist swing

Very similar to *Model 3*, the shape deforming, fixing and recovery were conducted by following the same procedures, and finally, the SMAFE could self-fitly worn on the wrist with a gradient geometry. As well, visual signal during wrist swing was detected and recorded by DMM6500.

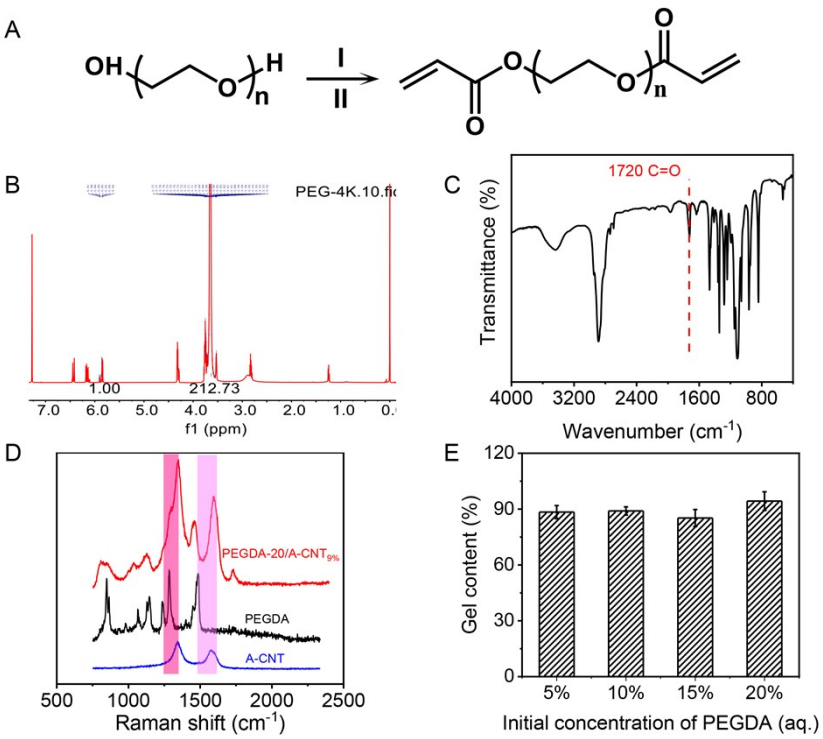

Fig. S1 (A) Synthetic route of PEGDA. Conditions: (I) K_2CO_3, CH_2Cl_2, room temperature. (II) Acrylylchloride, 48 h. (B) ^1H NMR spectrum of $PEGDA_{4000}$ in $CDCl_3$. (C) FT-IR spectrum of $PEGDA_{4000}$. (D) Raman spectra of PEG-20/$CNT_{9\%}$, PEGDA, A-CNT. (E) Gel contents of the prepared aerogels with different initial concentrations of PEGDA (aq.).

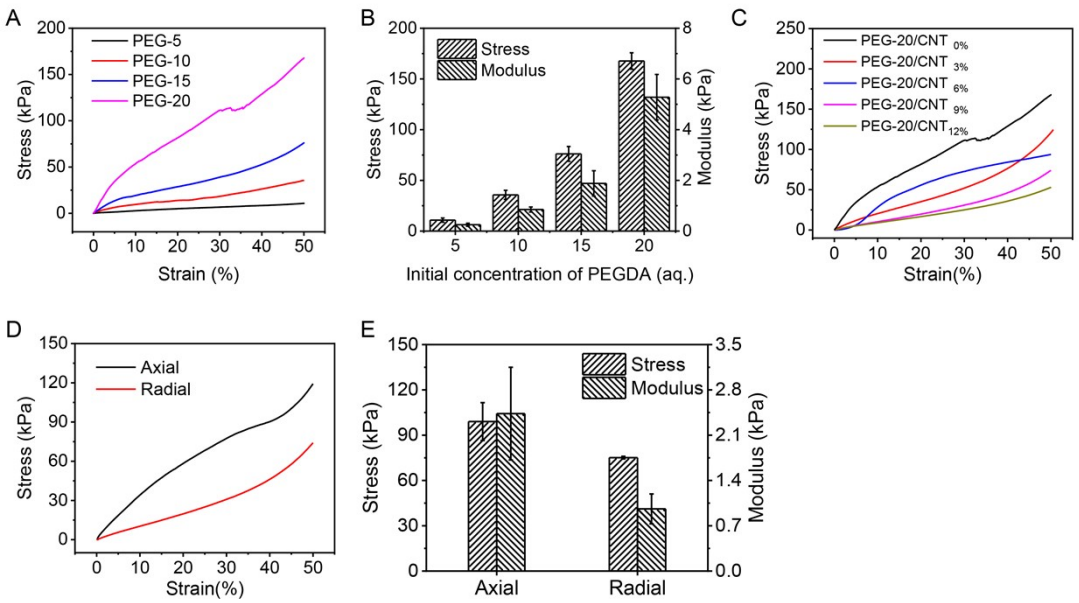

Fig. S2 (A-B) Stress-strain curves (A) and data of compressive strength and modulus (B) of the aerogels from different initial concentrations of PEGDA (aq.) (5%, 10%, 15% and 20%) obtained from compression testing. The compressive strain was set as 50%. (C) Stress-strain curves of the aerogels with different adding amounts of A-CNTs. (D-E) Stress-strain curves (D) and data of compressive strength and modulus (E) in different directions (radial and axial).

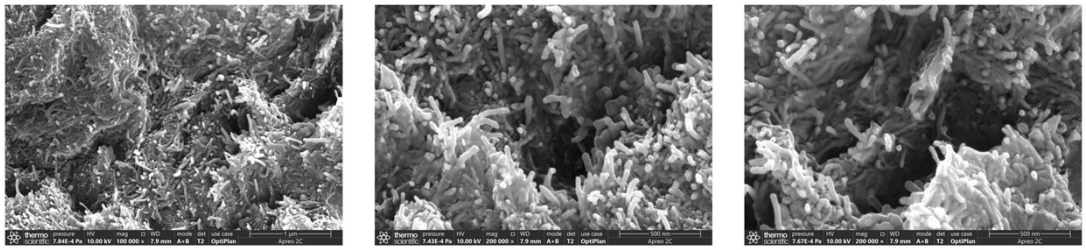

Fig. S3 Distribution of A-CNTs on the cell walls of the microporous aerogels obtained from SEM.

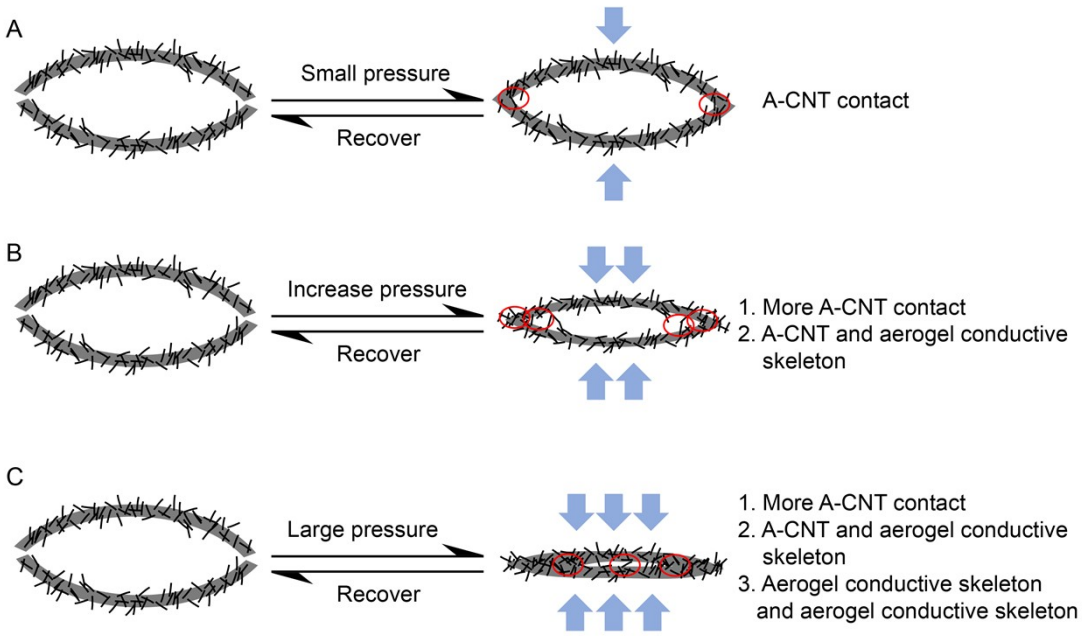

Fig. S4 Schematic illustration for the working mechanism of the aerogel sensor.

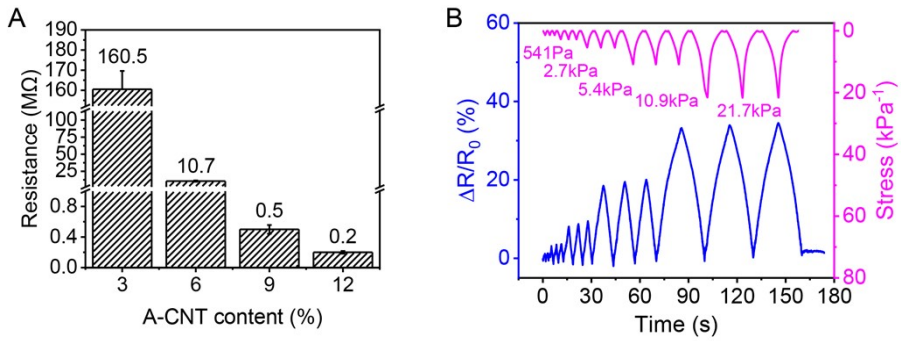

Fig. S5 (A) Resistance of the composite aerogels with different adding amounts of A-CNTs. (B) Resistance change of the conductive aerogels at low pressures.

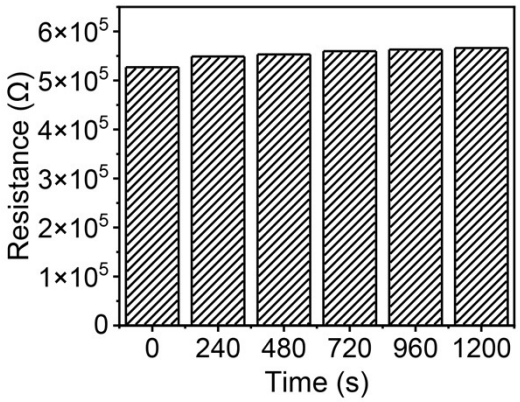

Fig. S6 Variation in resistance of the SMAFE in 2500-cycle compressing test at 10% strain.

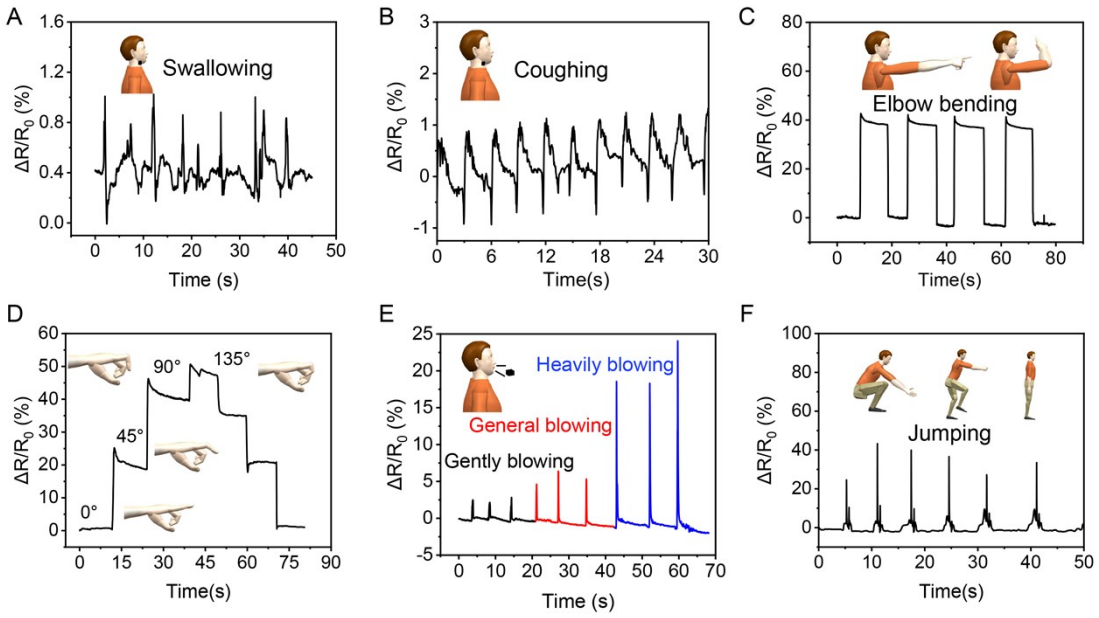

Fig. S7 Supplementary sensing scenarios of the SMAFE. (A) Swallowing. (B) Coughing. (C) Elbow bending. (D) Figure bending (0°,45°,90°,135°). (E) Blowing. (F) Jumping.

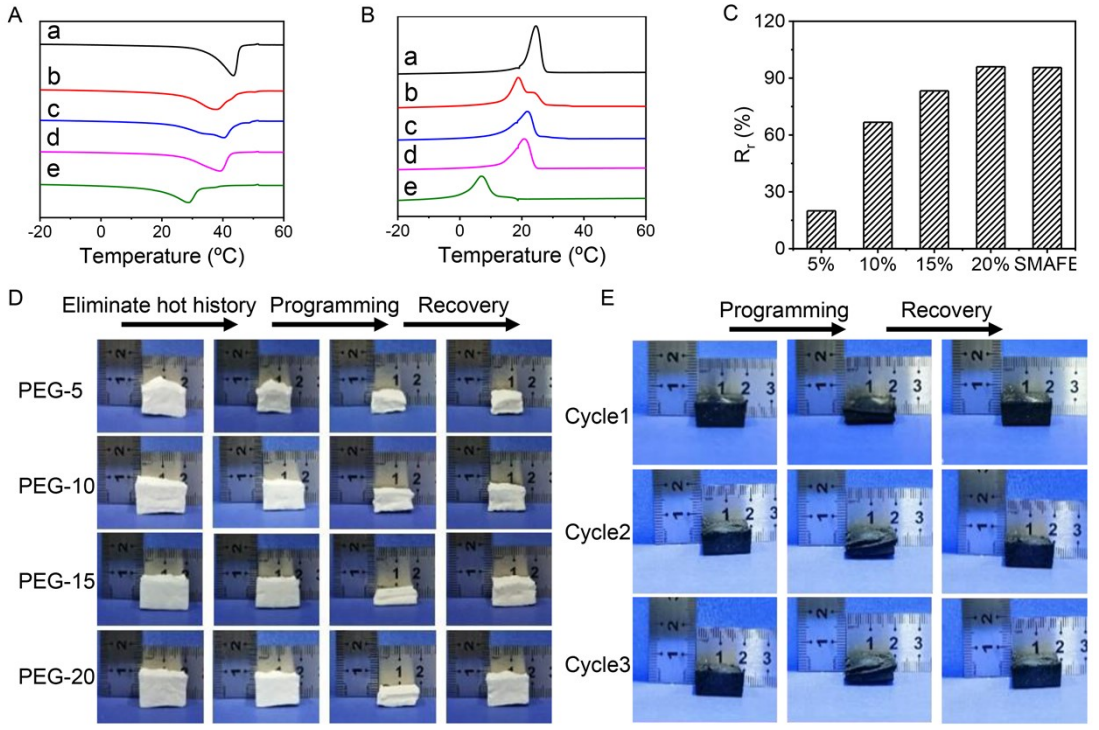

Fig. S8 Investigation of shape-memory properties of the aerogels. (A-B) DSC curves of the series of aerogels in cooling run (A) and subsequent heating run (B) at a rate of 5 °C/min (a-e are PEG-5, PEG-10, PEG-15, PEG-20, and PEG-20/$CNT_{9\%}$ respectively). (C) Shape recovery ratio (R_r) of the aerogels from different initial concentrations of PEGDA (aq.). Here, sample for SMAFE was PEG-

20/$CNT_{9\%}$. (D) Photos showing shape-memory process (programming and recovery) of the aerogels from different initial concentrations of PEGDA (aq.). (E) Photos showing three successive shape-memory properties of the SMAFE (PEG-20/$CNT_{9\%}$).

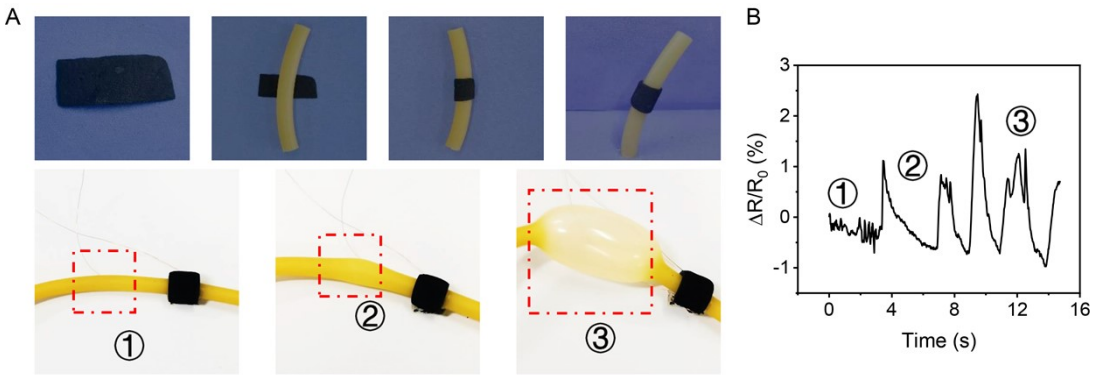

Fig. S9 Demonstration of the capacity of the SMAFE in reprogramming and worn on a hose by shape fixing (A) to examine the inside pressure (B), without any sacrifice of sensing performance at each state.

Table S1. Details of the raw materials for preparing the series of aerogels

Sample	$PEGDA_{4000}$ (g)	$PEGDA_{600}$ (g)	3%A-CNTs (mL)	H_2O (mL)	4%APS (μL)	TEMED (μL)
5%PEGDA(aq.)	0.525	0.225	0	15	500	50
10%PEGDA(aq.)	1.05	0.45	0	15	500	50
15%PEGDA(aq.)	1.575	0.675	0	15	500	50
20%PEGDA(aq.)	2.1	0.9	0	15	500	50
PEG-20/$CNT_{3\%}$	2.1	0.9	3	12	500	50
PEG-20/$CNT_{6\%}$	2.1	0.9	6	9	500	50
PEG-20/$CNT_{9\%}$	2.1	0.9	9	6	500	50
PEG-20/$CNT_{12\%}$	2.1	0.9	12	3	500	50

Table S2. Comparison of the detection range of porous materials in recent years

Materials	Minimum detection limit	Maximum detection limit	Refs
PEGDA/A-CNTs Aerogel	0.5 kPa	1200 kPa	This work
MXene/PANI/Bacterial Cellulose Aerogel	0.1 kPa	68.18 kPa	1
CNT sponge	2.2 kPa	5470 kPa	2
Silk Fibroin-MXene Composite Foams	0.071kPa	2 kPa	3
MXene@carboxylated CNT/carboxymethyl chitosan Aerogel	2.9 kPa	80.6 kPa	4
Porous PDMS	3 kPa	20 kPa	5
AgNW/Nanofibrillated cellulose Aerogel	0.5 kPa	8 kPa	6
MXene-Based Aerogel	0.06 kPa	66.98 kPa	7
PINF/MXene Aerogel	0.01 kPa	85.21 kPa	8
Aramid Nanofibers/ MXene Aerogel	0.1 kPa	5 kPa	9
Carbon Aerogel	-	16.89 kPa	10
Graphene Aerogel	0.01 kPa	10 kPa	11
Carbon Aerogel	-	10 kPa	12

Supplementary References

1. H. Zhi, X. Zhang, F. Wang, P. Wan and L. Feng, *ACS Appl. Mater. Interfaces,* 2021, **13**, 45987- 45994.
2. F. Xue, H. Zheng, Q. Peng, Y. Hu, X. Zhao, L. Xu, P. Li, Y. Zhu, Z. Liu and X. He, *Mater. Horiz.*, 2021, **8**, 2260-2272.
3. M. Bandar Abadi, R. Weissing, M. Wilhelm, Y. Demidov, J. Auer, S. Ghazanfari, B. Anasori, S. Mathur and H. Maleki, *ACS Appl. Mater. Interfaces*, 2021, **13**, 34996-35007.
4. Z. Yang, H. Li, S. Zhang, X. Lai and X. Zeng, *Chem. Eng. J.*, 2021, **425**, 130462.
5. M. Amit, R. K. Mishra, Q. Hoang, A. M. Galan, J. Wang and T. N. Ng, *Mater. Horiz.*, 2019, **6**, 604-611.
6. R. Cheng, J. Zeng, B. Wang, J. Li, Z. Cheng, J. Xu, W. Gao and K. Chen, *Chem. Eng. J.*, 2021, **424**, 130565.
7. D. Jiang, J. Zhang, S. Qin, Z. Wang, K. A. S. Usman, D. Hegh, J. Liu, W. Lei and J. M. Razal, *ACS Nano*, 2021, DOI: 10.1021/acsnano.0c09959.
8. H. Liu, X. Y. Chen, Y. J. Zheng, D. B. Zhang, Y. Zhao, C. F. Wang, C. F. Pan, C. T. Liu and C. Y. Shen, *Adv. Funct. Mater.*, 2021, **31**, 2008006.

9. L. Wang, M. Zhang, B. Yang, J. Tan and X. Ding, *ACS Nano*, 2020, **14**, 10633-10647.
10. Z. Chen, H. Zhuo, Y. Hu, H. Lai, L. Liu, L. Zhong and X. Peng, *Adv. Funct. Mater.*, 2020, **30**, 1910292.
11. G. Zu, K. Kanamori, K. Nakanishi, X. Lu, K. Yu, J. Huang and H. Sugimura, *ACS Appl. Mater. Interfaces*, 2019, **11**, 43533-43542.
12. Z. Chen, Y. Hu, H. Zhuo, L. Liu, S. Jing, L. Zhong, X. Peng and R. C. Sun, *Chem. Mater.*, 2019, **31**, 3301-3312.